Geophys. J. Int. (2005) **161,** 179–190 doi: 10.1111/j.1365-246X.2005.02583.x

A viscoelastic damage rheology and rate- and state-dependent friction

Vladimir Lyakhovsky,[1] Yehuda Ben-Zion[2] and Amotz Agnon[3]

[1] *Geological Survey of Israel, Jerusalem* 95501, *Israel. E-mail: vladi@geos.gsi.gov.il*
[2] *Department of Earth Sciences, University of Southern CA, Los Angeles CA* 90089-0740, *USA. E-mail: benzion@usc.edu*
[3] *Institute of Earth Sciences, Hebrew University of Jerusalem, Jerusalem* 91904, *Israel. E-mail: amotz@cc.huji.ac.il*

Accepted 2005 January 13. Received 2004 December 9; in original form 2004 April 26

SUMMARY

We analyse the relations between a viscoelastic damage rheology model and rate- and state-dependent (RS) friction. Both frameworks describe brittle deformation, although the former models localization zones in a deforming volume while the latter is associated with sliding on existing surfaces. The viscoelastic damage model accounts for evolving elastic properties and inelastic strain. The evolving elastic properties are related quantitatively to a damage state variable representing the local density of microcracks. Positive and negative changes of the damage variable lead, respectively, to degradation and recovery of the material in response to loading. A model configuration having an existing narrow zone with localized damage produces for appropriate loading and temperature–pressure conditions an overall cyclic stick–slip motion compatible with a frictional response. Each deformation cycle (limit cycle) can be divided into healing and weakening periods associated with decreasing and increasing damage, respectively. The direct effect of the RS friction and the magnitude of the frictional parameter a are related to material strengthening with increasing rate of loading. The strength and residence time of asperities (model elements) in the weakening stage depend on the rates of damage evolution and accumulation of irreversible strain. The evolutionary effect of the RS friction and overall change in the friction parameters ($a - b$) are controlled by the duration of the healing period and asperity (element) strengthening during this stage. For a model with spatially variable properties, the damage rheology reproduces the logarithmic dependency of the steady-state friction coefficient on the sliding velocity and the normal stress. The transition from a velocity strengthening regime to a velocity weakening one can be obtained by varying the rate of inelastic strain accumulation and keeping the other damage rheology parameters fixed. The developments unify previous damage rheology results on deformation localization leading to formation of new fault zones with detailed experimental results on frictional sliding. The results provide a route for extending the formulation of RS friction into a non-linear continuum mechanics framework.

Key words: cracked media, damage, earthquakes, fractures, friction, rheology.

1 INTRODUCTION

Brittle rock deformation is associated with fracture and friction processes. Fracture is dominant in deformation of rock without a pre-existing macroscopic failure zone, while friction is dominant in situations with existing sliding surfaces. At present, the most detailed description of rock friction is provided by the rate- and state-dependent (RS) friction (e.g. Dieterich 1979, 1981; Rice & Ruina 1983; Ruina 1983; Linker & Dieterich 1992). This framework accounts for the evolution of frictional strength as a function of slip, slip-velocity, normal stress and state variables that characterize properties of the sliding surfaces.

Dieterich (1972, 1978) performed frictional experiments with different values of normal stress, and hold times up to 10^5 s and described the increase of the static coefficient of friction f_s with time as

$$f_s = f_0 + A \log_{10}(1 + Bt), \tag{1a}$$

where t is the duration of the hold time in seconds, $f_0 \approx 0.6$–0.8, $A \approx (1$–$3)10^{-2}$ and $B \approx 1$–$2\ \mathrm{s}^{-1}$. The latter provides a timescale for the evolution of the static friction coefficient. The results were interpreted (e.g. Dieterich & Kilgore 1996; Scholz 2002) as representing enlargement of the real contact area with time as a result of indentation creep around geometrical asperities. Dieterich (1979, 1981),

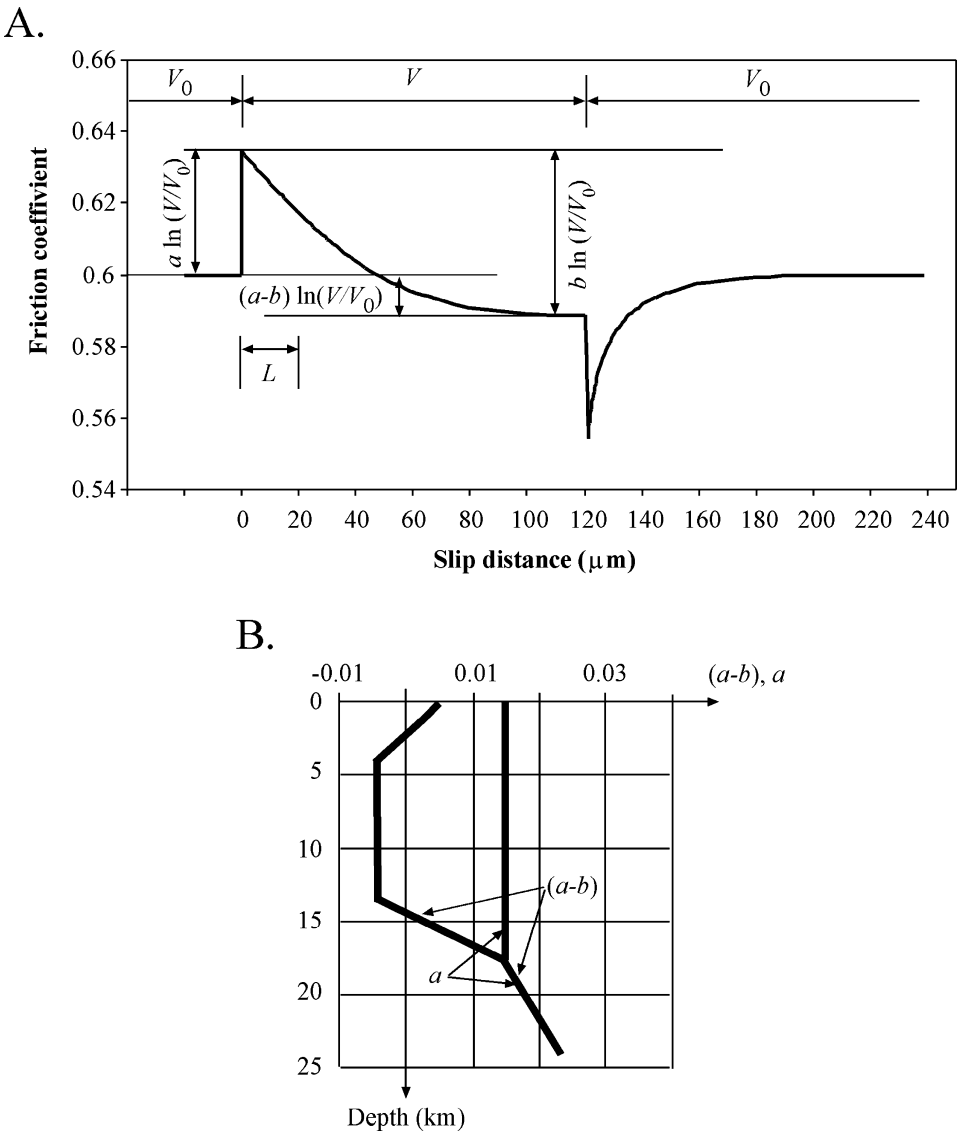

Figure 1. A diagram illustrating the main features of rate- and state-dependent friction in laboratory experiments. Panel A shows the response to velocity jumps from $V_0 = 1$ μm s^{-1} to $V = 10$ μm s^{-1}. The coefficient of friction is calculated according to the Dieterich law (eq. 2 from Marone 1998) with the following representative values for the seismogenic zone: $a = 0.015$, $b = 0.02$, $L = 20$ μm. Panel B shows depth variation of the frictional a and b parameters (modified from Rice 1993).

Ruina (1983) and others interpreted results of additional laboratory friction experiments involving hold times of the loading system and jumps in sliding velocities in terms of RS friction.

The basic aspects of the RS friction are illustrated in Fig. 1(a). An abrupt change in the loading velocity from V_0 to V produces a direct change to the friction coefficient with the same sign of the velocity change and amplitude $a \cdot \log(V/V_0)$. This is followed by an evolutionary effect with an opposite sign and amplitude $b \cdot \log(V/V_0)$ over a characteristic slip distance L. The dependency of the friction coefficient f on slip velocity and slip history is represented through an evolving state variable θ:

$$f = f_0 + a \ln\left(\frac{V}{V_0}\right) - b \ln\left(\frac{V_0\theta}{L}\right). \tag{1b}$$

There are several experimentally derived versions of the state evolution law (see Marone 1998, for review). During a steady-state sliding with constant velocity and slip distances larger than L, the state variable approaches asymptotically the value $\theta = L/V$ for the different evolution laws and the steady-state dependency of the friction coefficient on the sliding velocity is

$$f_{ss} = f_0 + (a - b) \ln\left(\frac{V}{V_0}\right). \tag{1c}$$

Dieterich (1979) interpreted L as representing the slip needed to renew surface contacts and thus L/V defines an average contact lifetime θ. Stesky *et al.* (1974), Blanpied *et al.* (1991, 1995) and Kilgore *et al.* (1993) measured the values of a and b for different pressure and temperature conditions. The observed ranges of parameters (sliding velocities, hold times, pressure, temperature, a, b, L) are summarized by Dieterich & Kilgore (1996), Marone (1998), Scholz (1998, 2002) and Ben-Zion (2003).The results indicate that $(a - b)$ changes sign from positive to negative at approximately 50 °C and back to positive at approximately 300 °C. Scholz (1998) noted that a temperature of 300 °C corresponds to the onset of crystal plasticity of quartz. If $(a - b)$ is positive, the overall change is referred to as velocity strengthening and the frictional response

favours stable sliding. On the other hand, if $(a - b)$ is negative the overall change is one of velocity weakening and the frictional response favours unstable sliding. The dependencies of $(a - b)$ on temperature and pressure can be converted to a function of depth (Fig. 1b), assuming representative changes of these state variables with depth (Blanpied *et al.* 1991; Rice 1993).

Linker & Dieterich (1992) investigated the effects of variable normal stress on the frictional resistance. They show that the change of the friction coefficient following a perturbation of normal stress is proportional to the logarithm of the normalized amplitude of the perturbation. The friction coefficient changes with the logarithm (base 10) of normal stress at a slope of 0.2. Richardson & Marone (1999) reported a similar tendency with a slightly higher slope between the friction coefficient and the logarithm of the normalized amplitude of the stress perturbation.

The RS friction provides a conceptual framework incorporating the main stages of an earthquake cycle on an existing fault plane (e.g. Tse & Rice 1986; Stuart & Tullis 1995; Ben-Zion & Rice 1997). However, this formulation does not provide a mechanism for possible evolution of the geometry of the slipping fault (or more generally fault network), and the related evolution of the elastic properties of the deforming fault zone(s) and surrounding rocks. Such processes are accounted for in damage rheology models that generalize Hookean elasticity to frameworks that relate an intensive damage state variable to evolving elastic properties (e.g. Lyakhovsky & Myasnikov 1985; Kachanov 1986; Krajcinovic 1996; Lyakhovsky *et al.* 1997a; Allix & Hild 2002). In continuum damage models, the damage state variable represents crack density in rock volumes large enough so that the distribution of internal flaws (microcracks in a laboratory specimen or small faults in a crustal domain) varies smoothly. Rabotnov (1988) related the damage variable to a reduction of the effective cross-section area that supports the load. Fiber-bundle models of damage (Newman & Phoenix 2001; Turcotte *et al.* 2003) share the same idea with torn fibers corresponding to cracks. Frictional frameworks have an analogous physical concept phrased in terms of the contact area. Sleep (1997, 1998) developed a mathematical formalism for RS friction using anisotropic damage tensor and connecting an evolving state variable with evolving damage. A general shortcoming of tensorial damage models (e.g. Ju 1990; Hansen & Schreyer 1994) is that they contain many more adjustable parameters than a scalar damage model. At present, it is impractical to constrain the parameters of the tensorial damage models with available data.

Lyakhovsky *et al.* (1997a) developed a scalar damage model that accounts for non-linear elasticity by adding to the free energy function of an elastic solid an additional second-order term and connecting the evolving elastic moduli to a single damage variable. Using general thermodynamic considerations (see Section 2) they derived a kinetic equation for the damage evolution that accounts for both degradation and healing as a function of the ongoing deformation and material properties. The energy stored in microcracks is related to degraded elasticity using a simple parametrization with an evolving damage state variable. Lyakhovsky *et al.* (1997a) constrained the model parameters by fracture and friction data, and explored the effect of damage-related evolving elasticity on time-dependent static friction. Hamiel *et al.* (2004) generalized the framework to a viscoelastic damage model with a power-law relation between the damage variable and effective elastic properties, and provided additional calibrations of model coefficients using stress–strain and acoustic emission data of triaxial laboratory experiments with Westerly granite and Berea sandstone. Ben-Zion *et al.* (1999), Lyakhovsky *et al.* (2001) and Ben-Zion & Lyakhovsky (2002, 2003) showed that the above damage rheology model can be used to study various aspects of crustal deformation associated with large earthquake cycles, including evolving fault zone geometries and material properties, evolving frequency-size and temporal statistics of earthquakes, accelerated seismic release, aftershocks and more. Various aspects of earthquakes have been studied also with RS friction (e.g. Dieterich 1994; Stein *et al.* 1997; Dieterich *et al.* 2000; Lapusta *et al.* 2000; Parsons *et al.* 2000; Ziv & Rubin 2003). In the following sections, we develop quantitative connections between observed phenomenology of RS friction, and the damage rheology model of Lyakhovsky *et al.* (1997a) and Hamiel *et al.* (2004).

2 A THERMODYNAMIC BASIS FOR DAMAGE RHEOLOGY

2.1 Evolving elasticity

The free energy of a damaged solid F may be written as

$$F = F(T, \varepsilon_{ij,} \alpha), \tag{2}$$

where T and ε_{ij} are the temperature and tensor of elastic strain, respectively, and α is a non-dimensional damage state variable.

Using the balance equations of energy and entropy accounting for irreversible changes of viscous deformation and material damage, the equation of Gibbs (1961) for evolving free energy, and the relation between the stress tensor, free energy and strain

$$\sigma_{ij} = \rho \frac{\partial F}{\partial \varepsilon_{ij}}, \tag{3}$$

the local entropy production as a result of damage evolution is represented as

$$\Gamma = \frac{1}{T} - \frac{\partial F}{\partial \alpha}\frac{d\alpha}{dt}. \tag{4}$$

The corresponding equation of damage evolution that provides a non-negative local entropy production has the form

$$\frac{d\alpha}{dt} = -C(\alpha, P, T)\frac{\partial F}{\partial \alpha}, \tag{5a}$$

where $C(\alpha, P, T)$ is a positive function of the state variables describing the rate of the damage process. In eq. (5a) the strain state variable is replaced by pressure that depends on α and strain. An actual use of eq. (5a) for the evolution of rock properties requires an explicit relation between the strain energy function and the damage variable. Using such a relation for basic physical conditions, Lyakhovsky *et al.* (1997a) derived an explicit equation for damage evolution in the form

$$\frac{d\alpha}{dt} = C_{\mathrm{d}}(\xi - \xi_0)I_2, \tag{5b}$$

where $\xi = I_1/\sqrt{I_2}$, $I_1 = \varepsilon_{kk}$ and $I_2 = \varepsilon_{ij}\varepsilon_{ij}$ (summation convention applied) are invariants of the strain tensor ε_{ij}, and the critical strain parameter ξ_0 is qualitatively similar to internal friction in Mohr–Coulomb yielding criteria. A state of strain ($\xi > \xi_0$) leads to material degradation (weakening of instantaneous elastic moduli) with a rate proportional to the second strain invariant multiplied by $(\xi - \xi_0)$. Similarly, a state of strain ($\xi < \xi_0$) results in material strengthening (healing of instantaneous elastic moduli) proportional to the same factors. Lyakhovsky *et al.* (1997a) assumed that during material degradation ($\xi > \xi_0$), the damage rate coefficient C is constant and labelled it C_d, while during material healing ($\xi < \xi_0$), C is an exponential function of α. The latter produces logarithmic healing as discussed in Section 2.4.

Additional quantitative results for various cases of 3-D deformation are given by Lyakhovsky *et al.* (1997a). The function $C(\alpha, P, T)$ that controls the kinetics of the damage evolution may be constrained by two different types of laboratory observations that account for the different physical processes associated with material degradation and healing. In Section 2.3, we consider laboratory constraints for the rate of damage increase (weakening). In Section 2.4, we discuss constraints for the rate of damage decrease (healing).

2.2 Viscoelastic damage model

For mathematical simplicity, Lyakhovsky *et al.* (1997a) ignored gradual accumulation of irreversible strain and assumed step-like increases of inelastic strain during macroscopic brittle failures associated with the lose of convexity of the free energy function. A shortcoming of this model is that after loading and full subsequent unloading prior to a macroscopic brittle failure, the strain returns to zero (possibly along a different path). This is not compatible with laboratory observations (e.g. Lockner 1993, 1998) of gradual inelastic strain accumulation as a result of microcrack growth and frictional sliding between grains before macroscopic failure.

In a Maxwell element, the strains are additive, so the total strain is that of the elastic component summed with that of the viscous component. In the damage rheology model, the elastic component is degrading and a plastic strain associated with this degradation should be accounted for. One can consider the rupture of bonds as the micromechanism for this degradation. For each bond that is ruptured, the elastic modulus diminishes and some elastic strain is converted to incremental permanent inelastic strain. This suggests for $d\alpha/dt > 0$ a proportionality between the rate of positive damage accumulation and the rate of gradual accumulation of the viscous component ε_{ij}^{v}:

$$\frac{d\varepsilon_{ij}^{v}}{dt} = C_{\mathrm{v}} \frac{d\alpha}{dt} \tau_{ij}, \tag{6}$$

where $C_{\mathrm{v}}(d\alpha/dt)$ is an effective damage-related ductile compliance or the inverse of an effective damage-related viscosity. As shown in the Appendix, energy conservation dictates that the value of C_{v} as a result of damage accumulation cannot exceed $[4(1-\alpha)^2\mu_0]^{-1}$. Yet, additional relaxation processes such as intracrystalline dislocation flow can produce higher C_{v} values. Hamiel *et al.* (2004) showed that a generalized version of the viscoelastic damage model with eq. (6) explains well observed stress–strain curves and acoustic emission data of laboratory experiments with Westerly granite and Berea sandstone.

2.3 Constraints for damage increase (weakening)

Laboratory experiments on rock fracture show an increase in the strength of intact rock with decreasing loading rate (Fig. 2). Lyakhovsky *et al.* (1997a) used fracture results of experiments with Westerly granite to constrain the damage rate parameter C_{d}. An assumed constant value of $C_{\mathrm{d}} = 3\ \mathrm{s}^{-1}$ provided a good fit to observed data for relatively high confining pressures (above 100 MPa), but significantly overestimated the strength of Westerly granite at low confining pressures. The simulated yielding envelope for different loading rates (fig. 6 of Lyakhovsky *et al.* 1997a) indicates that the damage rate parameter C_{d} should increase with decreasing confining pressure. Using the viscoelastic version of the damage rheology model with $C_{\mathrm{v}} = 3\ 10^{-5}\ \mathrm{MPa}^{-1}$ (Hamiel *et al.* 2004), we searched for a functional dependency of C_{d} that will allow us to fit the strength

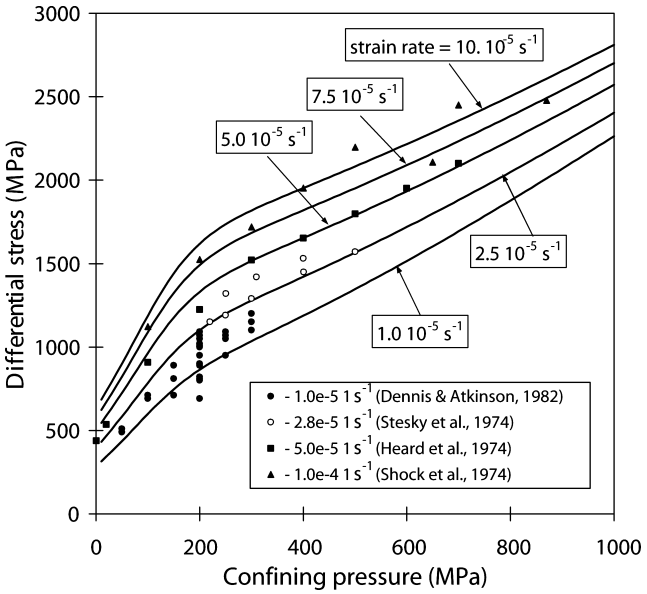

Figure 2. Experimentally observed yielding stress for Westerly granite under different confining pressure and loading rate (symbols). The lines give simulated yielding stress for the damage model parameters $\xi_0 = -0.8$, $C_{\mathrm{v}} = 3\ 10^{-5}\ \mathrm{MPa}^{-1}$ and C_{d} shown in Fig. 3.

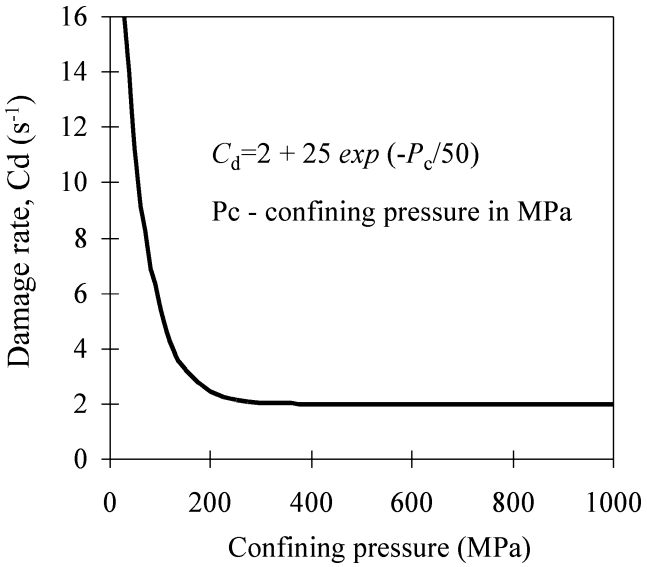

Figure 3. Damage rate parameter C_{d} versus confining pressure used for simulating the yielding envelope for Westerly granite shown in Fig. 2.

of Westerly granite measured for different confining pressures and strain rates (Fig. 2). A pressure-dependent C_{d} that varies exponentially with a characteristic scale of 50 MPa (Fig. 3) provides a good fit to the observed data. The resulting C_{d} is approximately constant for pressures above 100 MPa, indicating that for simulations of fracture processes in the seismogenic zone (i.e. at depth larger than 3–5 km) the damage rate parameter may be taken as constant. It should also be noted that the dependency of the yielding stress on the rate of loading is relatively weak, approximately a factor of 2 for an order of magnitude change in the loading rate. In a later section, we discuss connections between changes of the yielding stress with strain rates and the direct effect of the RS friction.

2.4 Constraints for damage decrease (healing)

Motivated by the observed logarithmic increase of the static coefficient of friction, Lyakhovsky *et al.* (1997a) used a damage-dependent function for the kinetics of healing of the form

$$C(\alpha) = C_1 \cdot \exp\left(\frac{\alpha}{C_2}\right), \quad \text{for } \frac{d\alpha}{dt} < 0, \tag{7}$$

where C_1 and C_2 are constants describing the rate of healing. With this expression, eq. (5a) for negative damage evolution (i.e. healing) under constant strain has the logarithmic solution

$$\alpha(t) = \alpha_0 - C_2 \cdot \ln\left[1 - \frac{C_1}{C_2} \cdot \exp\left(\frac{\alpha_0}{C_2}\right) \cdot \frac{\partial F}{\partial \alpha} \cdot t\right] \tag{8}$$

The damage decrease in eq. (8) leads to a logarithmic recovery of material strength in time, in agreement with the observed time-dependent logarithmic healing of the static coefficient of friction. A comparison between eqs (8) and (1a) indicates that the timescale in the frictional experiments of Dieterich (1972, 1978) are related to the damage rheology parameters as

$$B = -\frac{C_1}{C_2} \cdot \exp\left(\frac{\alpha_0}{C_2}\right) \cdot \frac{\partial F}{\partial \alpha} \approx \frac{C_1}{C_2} \cdot \exp\left(\frac{\alpha_0}{C_2}\right) \cdot \varepsilon_{\mathrm{CMP}}^2, \tag{9}$$

where $\varepsilon_{\mathrm{CMP}}$ is the compaction strain as a result of the imposed loading.

3 ANALYTICAL RESULTS FOR UNIFORM DAMAGE EVOLUTION IN A NARROW BAND

Our previous work was concerned in general with the evolution of a spatially heterogeneous region. Frictional processes apply where highly damaged regions form narrow bands within the fractured body. Here, we analyse analytically deformation processes associated with a uniform narrow damage zone between two moving elastic blocks that transmit shear stress (τ) to the damage zone (Fig. 4).

3.1 Deformation cycles and phases

The material in the damage zone is subjected to a constant compacting strain and increasing shear strain as a result of the motion of the outer elastic blocks. The total shear strain (ε) of the damage zone is written as a sum of the elastic reversible component ε_{e} and irreversible component (viscous and/or plastic) ε_{v}

$$\varepsilon = \varepsilon_{\mathrm{v}} + \varepsilon_{\mathrm{e}}. \tag{10}$$

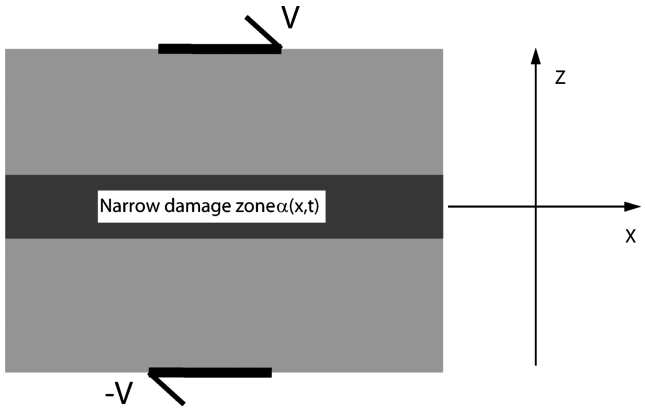

Figure 4. A 1-D model of an infinite damaged strip with a thickness $2h$ between elastic blocks with width $L \gg h$ and far-field velocity V.

In this section, the viscous strain ε_{v} is calculated with a constant Newtonian viscosity η to obtain a basic analytical understanding of the behaviour of the system. In the next section, we calculate the damage-related irrecoverable strain numerically using eq. (6) for the definition of the effective viscosity. For the case of a uniform damage zone and constant volumetric strain, the free energy (2) is

$$F = \mu_\alpha \left(\varepsilon_{\mathrm{e}}^2 - \varepsilon_{\mathrm{cr}}^2\right), \tag{11}$$

where the shear modulus $\mu_\alpha = \mu_0 (1 - \alpha)$ depends on the damage variable α and the critical strain $\varepsilon_{\mathrm{cr}}$ separates states of material degradation from healing. The linear relation between the damage variable and shear modulus is a 1-D approximation of the non-linear expressions for the effective elastic moduli of a damaged rock in 3-D (Lyakhovsky *et al.* 1997b). The threshold parameter $\varepsilon_{\mathrm{cr}}$ replaces the critical strain invariant ratio ξ_0 in the general 3-D formulation of Lyakhovsky *et al.* (1997a) leading to eq. (5b), where ξ_0 defines the neutral state of strain between healing and degradation.

The elastic shear strain in the damage zone is equal to the gradient of the difference between the total displacement u and the viscous displacement u_{v} in the zone

$$\varepsilon_{\mathrm{e}} = \frac{1}{2}\frac{\partial(u - u_{\mathrm{v}})}{\partial z}. \tag{12}$$

Substituting eq. (12) into the energy eq. (11) and using the constitutive relation (3), leads to a relation between the shear stress and the displacement components in the damage zone

$$\tau = \mu_\alpha \frac{\partial(u - u_{\mathrm{v}})}{\partial z}. \tag{13}$$

In the simple case of uniform damage, eqs (5a) and (5b) for damage evolution reduce to

$$\frac{d\alpha}{dt} = C(\alpha, P)\left[\varepsilon_{\mathrm{e}}^2 - \varepsilon_{\mathrm{cr}}^2\right], \tag{14}$$

where for healing states ($d\alpha/dt < 0$), $C(\alpha, P)$ is given by eq. (7) and for weakening states ($d\alpha/dt > 0$) it is given by the pressure-dependent $C_{\mathrm{d}}(P)$ of Fig. 3. The dilation strain is represented here by the pressure for convenience in application of the results to experimental data.

The solution to the elastodynamic problem inside the elastic blocks relates the shear stress τ_{h} and displacement u_{h} at the interfaces between the blocks and the damage zone as

$$\tau_{\mathrm{h}}(t) = \mu\left(\frac{Vt - u_{\mathrm{h}}(t)}{L} - \frac{1}{V_S}\frac{du_{\mathrm{h}}(t)}{dt}\right) \tag{15}$$

where L, μ and V_S are the width, shear modulus and shear wave velocity of the blocks, respectively. The first term on the right side of eq. (15) corresponds to quasi-static stress associated with slow motion. The second term, referred to as radiation damping, gives the change of stress associated with a plane shear wave propagating normal to the interface.

To obtain an analytical solution for the slow quasi-static evolution of the homogeneous damage zone, we approximate the displacement inside the zone by a linear function of the coordinate z (uniform strain). With this, the shear modulus and strain depend only on time, $\varepsilon = \varepsilon(t) = (u - u_{\mathrm{v}})/h$ and $\mu_\alpha = \mu_\alpha(t)$. Ignoring the radiation damping term, eqs (10)–(15) are reduced after some manipulations to a set of two coupled equations for ε_{e} and μ_α:

$$\begin{aligned}
\frac{d\mu_\alpha}{dt} &= -\mu_0 C(\alpha)\left[\varepsilon_{\mathrm{e}}^2 - \varepsilon_{\mathrm{cr}}^2\right], \\
\frac{d\varepsilon_{\mathrm{e}}}{dt} &= \frac{h\mu}{h\mu + L\mu_\alpha}\left[\frac{L}{h}\frac{\mu_0}{\mu}\varepsilon_{\mathrm{e}} C(\alpha)\left(\varepsilon_{\mathrm{e}}^2 - \varepsilon_{\mathrm{cr}}^2\right) + \frac{V}{h} - \frac{\mu_\alpha \varepsilon_{\mathrm{e}}}{\eta}\right].
\end{aligned} \tag{16}$$

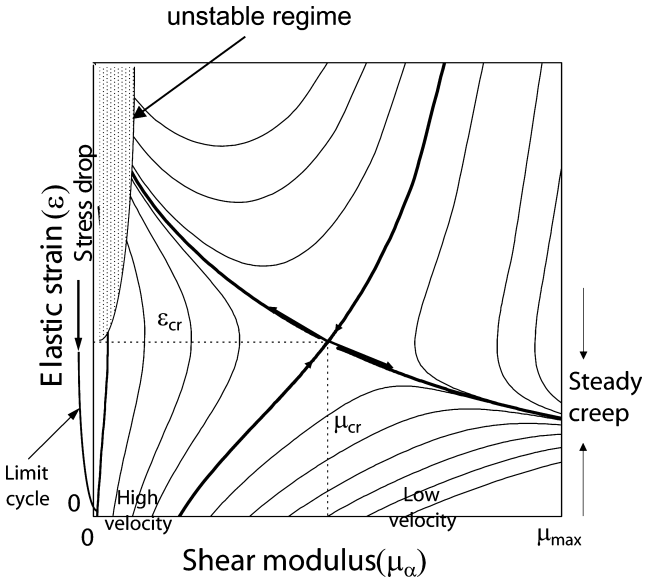

Figure 5. A phase-plane diagram for the evolution of a homogeneous damage zone.

The set (16) has an unstable stationary solution (a saddle point) of the form

$$\varepsilon_e = \varepsilon_{cr},$$

$$\mu_\alpha = \tfrac{V\eta}{h\varepsilon_{cr}}. \qquad (17)$$

The solution at point (17) and trajectories of the quasi-static evolution of the homogeneous damaged zone associated with the set (16) are illustrated by a phase plane shown in Fig. 5. For relatively low velocity of the bounding blocks, thick damage zone and low viscosity, there is a regime of steady creep. In this case, the healing process and the viscous stress relaxation are such that the elastic strain does not achieve the critical value associated with the onset of damage increase. This type of behaviour is likely to be dominant at high temperatures below the seismogenic zone. For relatively high velocity of the bounding blocks, thin damage zone and high viscosity, the elastic deformation may overcome its critical value and the damage level increases leading to a stress drop. This type of behaviour can be dominant at low temperatures that generally exist in the seismogenic zone.

The shaded area in the phase plane (Fig. 5) represents the zone where the quasi-static solution becomes unstable and a dynamic stress drop occurs. The dynamic stress drop (not analysed here) produces a reduction of the elastic strain in a rapid process during which the shear modulus remains very low. The brittle failure leads to an abrupt increase of plastic deformation that corresponds to slip in simpler models with planar faults. We assume that during brittle failure the deviatoric stress drops locally to zero leaving only the volumetric component. This is supported by laboratory experiments (e.g. Brune *et al.* 1993), theoretical models (e.g. Heaton 1990; Andrews & Ben-Zion 1997) and a variety of geophysical observations (see Ben-Zion 2001 for a summary). After the failure, the stress conditions favour healing and that stage lasts until the elastic strain reaches again the critical level and a new cycle begins.

Fig. 6 shows calculated damage and stress evolution during the discussed cycle. It can be shown that the topology of the quasi-static solution and existence of a limit cycle are general features of the damage rheology model and do not depend on the type of viscosity used to describe the inelastic strain. Note that the transition to

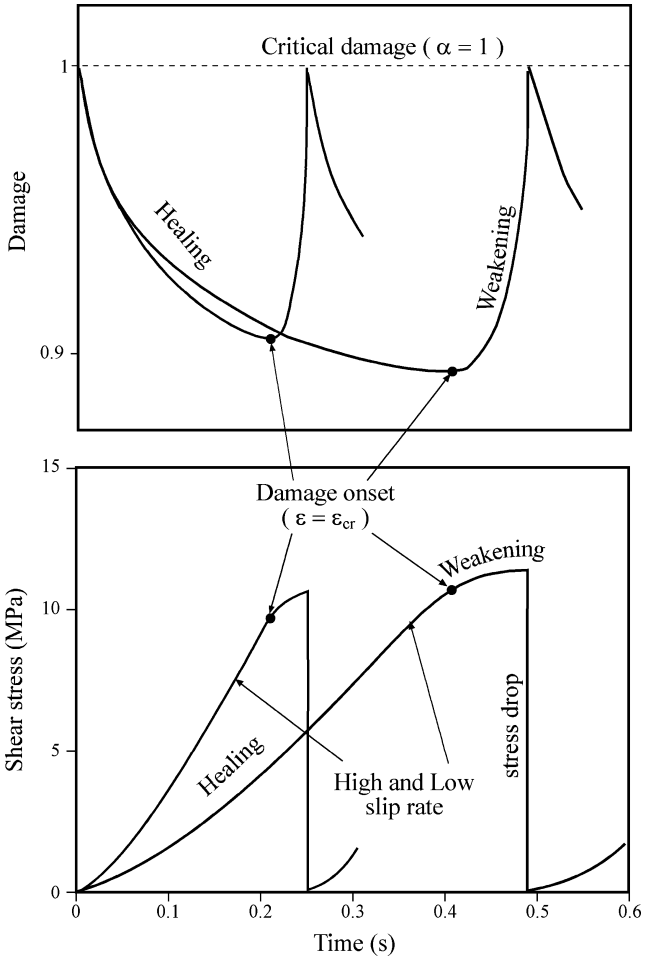

Figure 6. Calculated changes of damage and stress during a deformation cycle with high (2 μm s^{-1}) and low (1 μm s^{-1}) slip rates. The thickness of the damage zone is $h = 1$ mm; the healing rate parameters are $C_1 = 0.03$, $C_2 = 10^{-12}$ 1/s; the shear modulus of the damage-free material is $\mu_0 = 10^{11}$ Pa; and normal loading is $\sigma_n = 10$ MPa.

steady-state flow on the right of Fig. 5 requires a truly ductile deformation. For each cycle between subsequent failures, the duration and the average stress depend on the rate of loading, the rate and type (Newtonian or damage-related) of the inelastic strain accumulation, and the damage-rheology parameters that control the rates of weakening and healing. As shown in Fig. 6, each deformation cycle includes the following three stages: gradual healing, gradual weakening and an abrupt stress drop. The durations of the healing and weakening stages are larger by many orders of magnitude than the duration of the stress drop. The average shear stress $\bar{\tau}$ during the cycle may be estimated by integrating over the healing and weakening stages, or by calculating a weighted sum of the average values of stress in the different stages. The latter is given by

$$\bar{\tau} = \frac{\tau_h T_h + \tau_w T_w}{T_c}, \qquad (18)$$

where τ_h, T_h and τ_w, T_w are the average shear stress and duration of the healing and weakening stages, respectively, and $T_c = T_h + T_w$ is the total duration of the cycle. The ratio of $\bar{\tau}$ to the normal stress provides an estimate of the effective friction coefficient. Similarly, the corresponding ratios of the different terms on the right side of eq. (18) divided by the normal stress provide estimates of the

contributions of the healing and weakening processes to changes of the friction coefficient, respectively.

3.2 Average stress during the healing phase

The system of eqs (16) may be further simplified assuming that the elastic blocks are much stiffer than the damage zone. Because during the healing period there is also no accumulation of inelastic strain, eqs (16) for the healing period become

$$\frac{d\alpha}{dt} = -C_1 \exp\left(\frac{\alpha}{C_2}\right)\cdot\left(\varepsilon_e^2 - \varepsilon_{cr}^2\right),$$
$$\frac{d\varepsilon_e}{dt} = \frac{V}{h}. \tag{19}$$

The solution to the set (19) is

$$\alpha(t) = -C_2 \ln\left[\frac{C_1}{C_2}\left(\frac{V^2 t^3}{3h^2} - \varepsilon_{cr}^2 t\right) + \exp\left(-\frac{1}{C_2}\right)\right],$$
$$\varepsilon_e = \frac{V}{h}t. \tag{20}$$

The second expression with $\varepsilon = \varepsilon_{cr}$ gives the duration of the healing period T_h,

$$T_h = \frac{\varepsilon_{cr} h}{V}. \tag{21}$$

The two deformation cycles in Fig. 6 differ by their duration associated with the inverse proportionality between the slip velocity and T_h. The average shear stress τ_h during the healing period can be calculated from

$$\tau_h = \frac{1}{T_h}\int_0^{T_h} 2\mu_\alpha \varepsilon_e(t)dt. \tag{22}$$

Substituting eqs (20) and (21) into eq. (22) gives

$$\tau_h = \frac{2\mu_0 V^2}{h^2 \varepsilon_{cr}}\int_0^{\frac{\varepsilon_{cr} h}{V}} t\left\{1 + C_2 \ln\left[\frac{C_1}{C_2}\left(\frac{V^2 t^3}{3h^2} - \varepsilon_{cr}^2 t\right) + \exp\left(-\frac{1}{C_2}\right)\right]\right\} dt. \tag{23}$$

According to the above analysis of the static friction, C_2 is small so the term $\exp(-1/C_2)$ can be neglected and the average shear stress τ_h may be approximated as

$$\tau_h = \frac{\mu_0 \varepsilon_{cr}}{2}\left[1 - C_2 \ln\left(V\frac{C_2}{hC_1}\right) + O(C_2)\right], \tag{24}$$

where $O(C_2)$ is a constant value of the order of C_2^2 or smaller. The natural scale for the velocity is $V_0 = hC_1/C_2$. Thus, the reference velocity used to describe the frictional data is related to the thickness of the deforming slip zone and the ratio of the damage rheology parameters C_1/C_2. Eq. (24) shows explicitly that the shear stress during the healing period decreases with the logarithm of sliding velocity V. The coefficient C_2 can be obtained from eq. (24) as

$$C_2 = -\frac{1}{\tau_h}\frac{\partial \tau_h}{\partial \ln(V)}. \tag{25}$$

Experimentally, this coefficient is of order 10^{-2}, supporting the simplification of eqs (23) to (24).

In Section 4, we will show that during the weakening stage, the only contribution to the average stress is associated with the direct effect $a\cdot \ln(V/V_0)$ of the RS friction. Thus, the decrease of the RS friction associated with the term $b\cdot \ln(V/V_0)$ is produced entirely during the healing phase of deformation and is associated with the time interval of that phase. The healing rate coefficients C_1 and C_2 introduced in eq. (7) can now be related to the experimental parameters of RS friction. Replacing the shear stress in eq. (18) with $b\cdot \ln(V/V_0)\cdot\sigma_n$ and approximating τ_h by $f_{ss}\sigma_n$ with a constant σ_n gives

$$C_2 = \frac{b}{f_{ss}}\frac{T_c}{T_h}. \tag{26}$$

The weight factor (T_c/T_h) in eq. (26) normalizes the contribution of the healing phase to strength according to eq. (18). Using eqs (9) and (26), the coefficient C_1 may be expressed in terms of the rate constant B determined in the frictional experiments (1a) and the damage parameter C_2 as

$$C_1 = -BC_2 \cdot \exp\left(\frac{-\alpha_0}{C_2}\right)\Big/\frac{\partial F}{\partial \alpha} \approx BC_2 \cdot \exp\left(\frac{-\alpha_0}{C_2}\right)\Big/\varepsilon_{CMP}^2, \tag{27}$$

where ε_{CMP}, defined in eq. (9), is the compaction strain as a result of the imposed loading.

3.3 Average stress during the weakening phase

The simulated yielding envelopes of Fig. 2 correspond to the peak stress of a rock that is initially damage-free ($\alpha = 0$) and cannot be applied directly to estimate the average stress during the weakening phase. The latter requires the appropriate value of α at the end of the healing phase and therefore simulations of entire deformation cycles. Following the cycles in Fig. 6, we perform a numerical integration assuming that the initial shear stress is zero and the damage zone is completely destroyed ($\alpha = 1$). We then calculate the damage decrease and the average stress during the healing period and the subsequent weakening period that ends with the next stress drop. Fig. 7 shows the calculated change of the average shear to normal stress ratio during the weakening period versus the logarithm of slip velocity. The results indicate that the calculated stress ratio can be fitted well by line with a positive slope a. The estimated slope of the

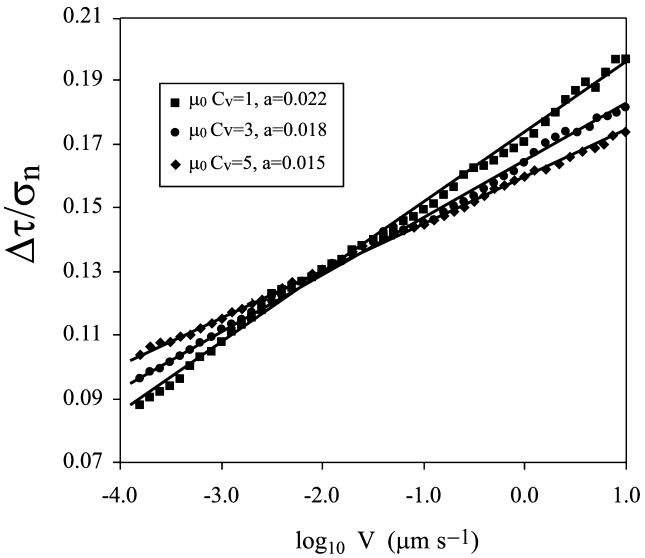

Figure 7. The average ratio between shear and normal stress during the weakening stage of deformation versus the logarithm of the slip rate for a homogeneous damage zone.

line defines a direct change of the friction coefficient with the same sign of the velocity change and an amplitude $a \cdot \log_{10}(v_2/v_1)$.

The obtained direct frictional parameter a depends on the value of α at the end of the healing phase and model parameters controlling the damage evolution during the weakening stage. With the healing parameters C_1 and C_2 of eqs (26), and (27) fixed, the direct frictional parameter a depends only on C_d and C_v. Larger C_v (or smaller effective viscosity) slightly increases the duration of the weakening stage (T_w) and significantly decreases the shear stress during a weakening stage, leading to a decrease of a. The a values in Fig. 7 decrease from 0.022 to 0.015 with increasing C_v from $\mu_0 C_v = 1$ to 5. This change of the calculated a values falls into the range of the temperature-related variations of a reported in laboratory observations and could be responsible for the transition from velocity weakening to strengthening. Larger C_d reduces both the duration of the weakening stage and the shear stress, leading to a decrease of the a parameter. A change of the C_d value by an order of magnitude generates (not shown here) an inverse change of the a value of approximately 0.003, from 0.022 to 0.025 or 0.019. However, the pressure-related increase of the damage rate parameter C_d at lower normal stresses (Fig. 3) is compensated by the decrease of elastic strain that reduces the rate of damage increase. Hence, the overall pressure dependency of the a value is very small as shown by numerical results discussed in the next section.

4 NUMERICAL RESULTS FOR SPATIALLY VARIABLE DAMAGE EVOLUTION

4.1 Model configuration

To account for spatial variations of the shear strain and stress components along the damage zone, we perform numerical simulations with heterogeneous distribution of damage in the x direction (Fig. 4). The inelastic strain prior to brittle failures is calculated using eq. (6) for the damage-related viscosity. During brittle failure, there are abrupt additions of incremental inelastic strain associated with local drops of the deviatoric stress component as discussed in Section 3.1. The most important change between the assumptions leading to the analytical results of Section 3 and the current numerical simulations is the nature of the interaction between the elastic blocks and the heterogeneous damage zone. Instead of eq. (15), here the shear stress at the interfaces between the elastic blocks and the damage zone is calculated using

$$\tau(x,t) = \frac{\mu}{\pi(1-\nu)} \int_{-\infty}^{\infty} \frac{\partial(Vt-u)}{\partial x} \frac{dx'}{x-x'} - \frac{\mu}{V_S}\frac{du}{dt}. \qquad (28)$$

In addition, we replace eq. (14) for a uniform damage evolution with the corresponding 3-D equation of Lyakhovsky *et al.* (1997a) given in eq. (5b). In the calculations below, we use $\xi_0 = -0.8$ following the laboratory-based estimates of Agnon & Lyakhovsky (1995), Lyakhovsky *et al.* (1997a) and Hamiel *et al.* (2004) for Westerly granite.

The shear stress (28) at the grid points along the damage zone is calculated using the trapezoidal rule for every interval except that containing the singular point $x = x'$. In the interval with a singular point, the principal value based on the Cauchy integral theorem is used. Combining the results of integration with the stress–strain relation

$$\tau(x,t) = \mu_\alpha(x,t)\frac{u-u_v}{h} \qquad (29)$$

lead to a linear system of equations for the displacement $\mu_\alpha(x, t)$, which is solved at every time step for a given shear modulus $\mu_\alpha(x, t)$. This method is a 1-D equivalent of the well-known boundary element method (BEM) that is usually applied for 2-D or 3-D elasticity. The kinetic equation for damage evolution and eq. (6) for irreversible strain accumulation are integrated explicitly in time. Comparisons of numerical runs with different initial random damage distributions along the strip show that, after several deformation cycles, a steady-state sliding is achieved and the macroscopic friction does not depend on the initial conditions. The frictional values and duration of the evolutionary stage depend slightly on the number of gridpoints, but the variations become negligible when a grid with several hundreds of points or more is used.

4.2 Simulation results

In the case of initially homogeneous damage, the numerical solution of eqs (28) and (29) gives the same results obtained for a homogeneous zone. However, random initial damage distribution in the damage zone leads to some spatially and temporally uncorrelated evolution of material elements. The applied stress on the elastic blocks that is required to obtain a constant slip velocity approaches a constant value that depends logarithmically on the block velocity and the normal stress (Fig. 8). An order of magnitude change in slip

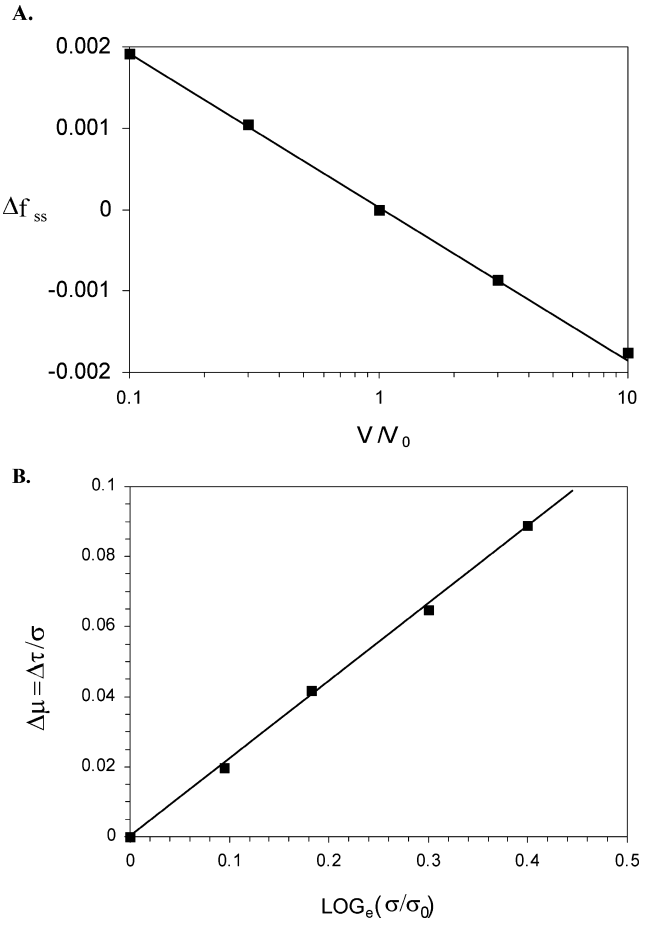

Figure 8. Results of numerical simulations for spatially variable damage evolution. Panel A gives the change of the steady-state friction coefficient versus slip rate. Panel B gives the change of steady-state friction as a function of normal stress. The results duplicate the logarithmic dependencies observed in laboratory rate- and state-dependent friction experiments.

velocity produces a change of approximately 0.02 in the steady-state coefficient of friction (squares in Fig. 8a). This numerical result confirms the expected relation between slip velocity and steady-state friction. Another set of numerical simulations reproduces the effect of normal stress variations on the steady-state frictional strength (Fig. 8b). In this set, we apply different changes of normal stress and keep all the other model parameters including slip velocity constant. The simulated increase of the steady-state friction with increasing normal stress is associated in our model with the fact that the damage evolution is proportional to $(\xi - \xi_0)$. The strain invariant ratio, $\xi = I_1/\sqrt{I_2}$, increases with decreasing confining pressure from $\xi = -\sqrt{3}$ for 3-D isotropic compaction to $\xi = 0$ for pure shear stress. Thus, under high confining pressure, the material healing is more efficient and the duration of the healing stage is longer than under lowered pressures.

Different types of frictional behaviour from velocity weakening to velocity strengthening can be reproduced by changing some model parameters (Fig. 9). In these simulations we apply a velocity step to the model with different rates of irreversible strain, changing C_v and keeping all other model parameters (including normal stress) constant. In agreement with the analytical and numerical results of the previous section, only the a value depends on the change in the rate of damage-related irreversible strain accumulation. The same b value was obtained for three different simulations with variable C_v values ($\mu_0 C_v = 1, 3, 5$). The resulting $a - b$ for low values of C_v ($\mu_0 C_v = 1$) is positive, corresponding to velocity strengthening. Model simulations with $\mu_0 C_v = 5$ show negative $a - b$ values, corresponding to velocity weakening. A neutral behaviour $a = b$ is also shown in Fig. 9 and is obtained for $\mu_0 C_v = 3$.

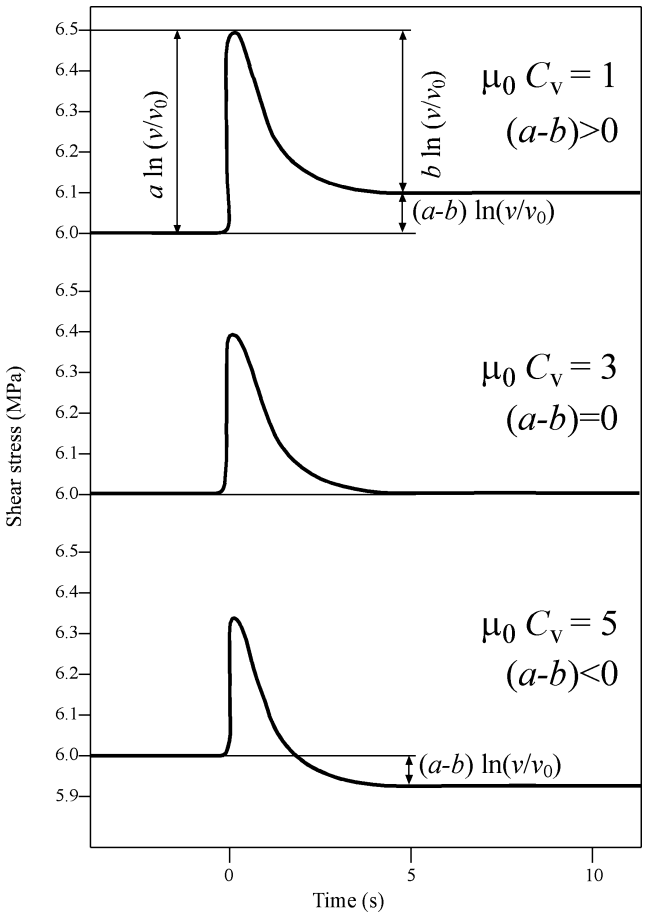

Figure 9. Results of numerical simulations with three different C_v values ($\mu_0 C_v = 1, 3, 5$). The calculations show a transition from velocity strengthening to velocity weakening with increasing C_v. The thickness of the damage zone is $h = 1$ mm; the healing rate parameters are $C_1 = 0.03$, $C_2 = 10^{-12}$ 1/s; the shear modulus of the damage-free material is $\mu_0 = 10^{11}$ Pa; and the normal loading $\sigma_n = 10$ MPa. These parameters are the same as in the model leading to Fig. 6.

5 DISCUSSION AND CONCLUSIONS

Brittle rock behaviour is often modelled by a rigid elastic–plastic solid that is governed by simple static/kinetic friction. The RS friction provides a framework that can be used to simulate important aspects of earthquake cycles, including stable slip, nucleation of instabilities, rupture propagation and healing. However, the RS formulation assumes that deformation at all stages occurs on well-defined frictional surfaces, and it does not provide a mechanism for understanding brittle deformation along zones with complex evolving geometrical and material properties (e.g. Andrews 1989; Ben-Zion & Rice 1995). Damage rheology models can account for these realistic aspects of rock deformation. Our previous studies on this topic (e.g. Lyakhovsky & Myasnikov 1985; Lyakhovsky *et al.* 1997a,b; Hamiel *et al.* 2004) focused primarily on applications of damage rheology for describing brittle rock deformation from the first yielding or onset of damage to the final macroscopic failure. Following Kachanov (1986), the damage state variable in our model represents the evolving elastic properties and is related to the density of crack population in a representative rock volume. We note, however, that direct relations between damage models and crack density are still not fully available (e.g. Katz & Reches 2004).

Lyakhovsky *et al.* (1997a) developed a thermodynamically based damage rheology model that provides a quantitative description of both fracturing (material degradation) and healing (material recovery) during irreversible deformation. Positive and negative changes of the damage state variable lead in the model to degradation and healing of the material, respectively. The latter was assumed by Lyakhovsky *et al.* (1997a) to be governed by exponential healing kinetics. This enables the damage model to reproduce the observed logarithmic increase of the static coefficient of friction. In the present work, we develop detailed connections between the phenomenology and parameters of the RS friction and the damage rheology model.

At a given compression, shear strain excess over a threshold value induces material degradation with a rate coefficient C_d of order 1 s^{-1}. Under lower strain, the damage heals at a rate proportional to $C_1 \exp(C_2\alpha)$ with coefficients C_1 and C_2 that depend weakly on rock type. For sufficiently high strain rate, there is a limit cycle response, with each deformation cycle divided into healing and weakening periods associated with decreasing and increasing damage, respectively. The rate of inelastic strain accumulation before the final brittle failure is proportional to the rate of damage increase multiplied by a coefficient C_v. Experimental results show that the yielding envelope under constant confining pressure increases with the strain rate. This is accounted for in our model by the coefficient C_d.

Using a simplified model with uniform damage evolution, we obtain analytically the following connections between parameters of the damage rheology model and those of the RS friction.

(i) The timescale in frictional experiments that governs the increase of the static coefficient of friction during hold time increases with increasing initial damage at the start of the hold period,

increasing C_1, decreasing C_2 and increasing compaction strain as a result of the imposed loading.

(ii) The reference velocity in the expressions describing the rate-state frictional results is proportional to the thickness of the deforming zone multiplied by the ratio of the healing parameters C_1/C_2.

(iii) The evolutionary frictional parameter b is proportional to C_2 multiplied by the steady-state friction coefficient f_{ss} and the relative duration of the healing stage of the deformation cycle.

Numerical simulations indicate that the direct frictional parameter a is inversely proportional to C_d and C_v. For a model with spatially variable properties, the damage rheology reproduces the logarithmic dependency of f_{ss} on the sliding velocity and normal stress. The transition from a velocity-strengthening to a velocity-weakening regime can be obtained by varying the parameter C_v and keeping the other damage rheology parameters fixed. Cases with C_v much larger than the shear compliance lead to $a < b$ and an overall velocity weakening, while small values of C_v give $a > b$ and velocity strengthening.

The effect of normal stress variation in RS frictional experiments is reproduced by our model with all parameters fixed and is solely associated with the critical strain parameter ξ_0 (eq. 5b). Linker & Dieterich (1992) reported a linear experimental relation between $\Delta\mu = \Delta\tau/\sigma$ and $\mathrm{LOG_e}(\sigma/\sigma_0)$ for normal stress variations up to 0.4 in logarithmic units (see their fig. 5). The corresponding simulated response of Fig. 8(b) indicates that the 3-D formulation of our model is to first order correct. The numerical modelling with heterogeneous damage and spatial averaging of stress shows similar results to the temporal averaging obtained analytically. This suggests that our multi-element system is ergodic.

Eqs (26) and (27) relate the healing parameters C_1 and C_2 introduced in eq. (7) to the static and steady-state friction coefficients. This allows us to estimate the values of C_1 and C_2 from the timescale B of the static RS frictional experiments and the parameter b of the dynamic friction experiments. Because b is $\sim 10^{-2}$, f_{ss} is $\sim$0.6–0.8, the duration of the healing stage (T_h) is longer than the weakening stage (T_w), and thus C_2 is between 10^{-1} and 10^{-2}. As shown in eq. (27), the value of the coefficient C_1 strongly depends on the value of the coefficient C_2. For $C_2 = 0.05$, $B \sim 1\ \mathrm{s}^{-1}$ and $\varepsilon_{CMP} \sim 10^{-2}$, the coefficient C_1 is $\sim 10^{-6}\ \mathrm{s}^{-1}$, while for $C_2 = 0.03$ and the other values as before C_1 is $\sim 10^{-12}\ \mathrm{s}^{-1}$. With these parameters, fault healing at a pressure of approximately 200 MPa is very fast during the initial few hours after an earthquake and the rate of healing significantly decreases with time. In the first case of $C_2 = 0.05$, the value of the damage variable 1 yr after the earthquake is expected to be $\sim$0.2, corresponding to $\sim$ 80 per cent of material recovery. In the second case of $C_2 = 0.03$, the material recovery over the same time is only $\sim$50 per cent. The material recovery will continue with a rate of approximately $10^{-2}\ \mathrm{yr}^{-1}$ as long as the loading conditions favour healing. It is important to obtain stronger constrains on the value of C_2 from future laboratory experiments, because small variations of C_2 lead to significant variations in the rate of material recovery and the rigidity of the fault zone. The parameters controlling the weakening stage of the deformation cycle are also not well resolved by the available laboratory data. For instance, the temperature dependency of the fracturing process expressed by $C_d(T)$ is not constrained. It is especially important to constrain the temperature and pressure dependency of the kinetic damage parameters in the semi-brittle regime.

A static friction proportional strictly to $\log(t)$ gives unbounded values for infinite time. A related problem emerges with the exponential form of healing in eq. (8). The damage variable approaches zero during a finite time and may even become negative. A power-law relation between the damage variable and elastic moduli in a viscoelastic version of our model (Hamiel *et al.* 2004) fixes this shortcoming. A transitional strain invariant ratio in the power-law damage model decreases and approaches $-\sqrt{3}$ and prevents further healing when α approaches zero. In the simulations presented here, the α values are relatively large (close to 1) and the cycle durations are small. In these conditions, the difference between the employed simplified damage rheology model and the power-law version of the model is negligible. However, the difference could be important for healing of pre-existing weak zones on geological timescales.

The analytical results discussed in this work do not incorporate changes in the second dimension along the fault and in the third dimension normal to the fault. Our theoretical results thus do not account for effects associated with general distributions of contact areas along the two fault dimensions and effects associated with a finite thickness of the fault zone (i.e. the existence of gouge).

ACKNOWLEDGMENTS

We thank Thorsten Becker and two anonymous reviewers for constructive reviews. The studies were supported by a grant of the US–Israel Binational Science Foundation, Jerusalem Israel (9800198) to VL, grants of the United States Geological Survey (02HQGR0047) and the Southern California Earthquake Center (based on National Science Foundation (NSF) cooperative agreement EAR-8920136 and United States Geological Survey cooperative agreement 14-08-0001-A0899) to YBZ, and a grant of International Association-European Community (INTAS-EU) (0748) to AA.

REFERENCES

Agnon, A. & Lyakhovsky, V., 1995. Damage distribution and localization during dyke intrusion, in *The physics and Chemistry of Dykes,* pp. 65–78, eds Baer, G. & Heimann A., Balkema, Brookfield.

Allix, O. & Hild, F., 2002. *Continuum damage mechanics of materials and structures,* Elsevier, p. 396. Amsterdam Holland.

Andrews, D.J., 1989. Mechanics of fault junctions, *J. geophys. Res.,* **94,** 9389–9397.

Andrews, D.J. & Ben-Zion, Y., 1997. Wrinkle-like slip pulse on a fault between different materials, *J. Geophys. Res.,* **102,** 553–571.

Ben-Zion, Y., 2001. Dynamic ruptures in recent models of earthquake faults, *J. Mech. Phys. Solids,* **49,** 2209–2244.

Ben-Zion, Y., 2003. Key formulas in earthquake seismology, in *International handbook of earthquake and engineering seismology,* Part B, pp. 1857–1875, Academic Press, (eds.) W.H.K. Lee, H. Kanamori, P.C. Jennings, and C. Kisslinger, San Diego, CA.

Ben-Zion, Y. & Lyakhovsky, V., 2002. Accelerating seismic release and related aspects of seismicity patterns on earthquake faults, *Pure and appl. Geophys.,* **159,** 2385–2412.

Ben-Zion, Y. & Lyakhovsky, V., 2003. A generalized law for aftershock rates in a damage rheology model, *EOS, Trans. Am. geophys. Un.,* **84**(46), F781.

Ben-Zion, Y. & Rice, J.R., 1995. Slip patterns and earthquake populations along different classes of faults in elastic solids, *J. geophys. Res.,* **100,** 12 959–12 983.

Ben-Zion, Y. & Rice, J.R., 1997. Dynamic simulations of slip on a smooth fault in an elastic solid, *J. geophys. Res.,* **102,** 17 771–17 784.

Ben-Zion, Y., Dahmen, K., Lyakhovsky, V., Ertas, D. & Agnon, A., 1999. Self-driven mode switching of earthquake activity on a fault system, *Earth planet. Sci. Lett.,* **172,** 11–21.

Blanpied, M.L., Lockner, D.A. & Byerlee, J.D., 1991. Fault stability inferred from granite sliding experiments at hydrothermal conditions, *Geophys. Res. Lett.,* **18,** 609–612.

Blanpied, M.L., Lockner, D.A. & Byerlee, J.D., 1995. Frictional slip of granite at hydrothermal conditions, *J. geophys. Res.,* **100,** 13 045–13 064.

Brune, J.N., Brown, S. & Johnson, P.A., 1993. Rupture mechanism and interface separation in foam rubber model of earthquakes: a possible solution to the heat flow paradox and the paradox of large over thrusts, *Tectonophysics,* **218,** 59–67.

Dieterich, J.H., 1972. Time-dependent friction in rocks, *J. geophys. Res.,* **77,** 3690–3697.

Dieterich, J.H., 1978. Time-dependent friction and the mechanics of stick–slip, *Pure appl. Geophys.,* **116,** 790–805.

Dieterich, J.H., 1979. Modeling of rock friction 1. Experimental results and constitutive equations, *J. geophys. Res.,* **84,** 2161–2168.

Dieterich, J.H., 1981. Constitutive properties of faults with simulated gouge, *Am. geophys. Un. Monogr.,* **24,** 103–120.

Dieterich, J.H., 1994. A constitutive law for rate of earthquake production and its application to earthquake clustering, *J. geophys. Res.,* **99,** 2601–2618.

Dieterich, J.H. & Kilgore, B.D., 1996. Imaging surface contacts; power law contact distributions and contact stresses in quarts, calcite, glass, and acrylic plastic, *Tectonophysics,* **256,** 219–239.

Dieterich, J.H., Cayol, V. & Okubo, P., 2000. The use of earthquake rate changes as a stress meter at Kilauea volcano, *Nature,* **408,** 457–460.

Gibbs, J.W., 1961. *The Scientific Papers, Thermodynamics,* Vol. 1, Dover, New York.

Hamiel, Y., Liu, Y., Lyakhovsky, V., Ben-Zion, Y. & Lockner, D., 2004. A visco-elastic damage model with application to stable and unstable fracturing, *Geophys. J. Int.,* **159,** 1155–1165.

Hansen, N.R. & Schreyer, H.L., 1994. A thermodynamically consistent framework for theories of elasticity coupled with damage, *Int. J. Solids Struct.,* **31,** 359–389.

Heaton, T.H., 1990. Evidence for and implications of the self-healing pulses of slip in earthquake rupture, *Phys. Earth planet. Int.,* **64,** 1–20.

Ju, J.W., 1990. Isotropic and anisotropic damage variables in continuum damage mechanics, *J. Eng. Mech.,* **116,** 2764–2770.

Kachanov, L.M., 1986. *Introduction to continuum damage mechanics,* Martinus Nijhoff Publishers, Boston, p. 135.

Katz, O. & Reches, Z., 2004. Microfracturing, damage, and failure of brittle granites, *J. geophys. Res.,* **109,** B01206, doi:10.1029/2002JB001961.

Kilgore, B.D., Blanpied, M.L. & Byerlee, J.D., 1993. Velocity dependent friction of granite over a wide range of conditions, *Geophys. Res. Lett.,* **20,** 903–906.

Krajcinovic, D., 1996. *Damage Mechanics,* Elsevier, Amsterdam.

Lapusta, N., Rice, J.R., Ben-Zion, Y. & Zheng, G., 2000. Elastodynamic analysis for slow tectonic loading with spontaneous rupture episodes on faults with rate- and state-dependent friction, *J. geophys. Res.,* **105,** 23 765–23 789.

Linker, M.F. & Dieterich, J.H., 1992. Effects of variable normal stress on rock friction: observations and constitutive equations, *J. geophys. Res.,* **97,** 4923–4940.

Lockner, D.A., 1993. Room temperature creep in saturated granite, *J. geophys. Res.,* **98,** 475–487.

Lockner, D.A., 1998. A generalized law for brittle deformation of Westerly granite, *J. geophys. Res.,* **103,** 5107–5123.

Lyakhovsky, V.A. & Myasnikov, V.P., 1985. On the behavior of visco-elastic cracked solid, *Physics of Solid Earth,* **4,** 28–35.

Lyakhovsky, V., Ben-Zion, Y. & Agnon, A., 1997a. Distributed damage, faulting and friction, *J. geophys. Res.,* **102,** 27 635–27 649.

Lyakhovsky, V., Reches, Z., Weinberger, R. & Scott, T.E., 1997b. Nonlinear elastic behavior of damaged rocks, *Geophys. J. Int.,* **130,** 157–166.

Lyakhovsky, V., Ben-Zion, Y. & Agnon, A., 2001. Earthquake cycle, fault zones and seismicity pattern s in a rheologically layered lithosphere, *J. geophys. Res.,* **106,** 4103–4120.

Marone, C., 1998. Laboratory-derived friction laws and their application to seismic faulting, *Ann. Rev. Earth. planet. Sci.,* **26,** 643–696.

Newman, W.I. & Phoenix, S.L., 2001. Time-dependent fiber bundles with local load sharing, *Phys. Rev. E.,* **63**(2), art. no. 021507.

Parsons, T., Toda, S., Stein, R.S., Barka, A. & Dieterich, J.H., 2000. Heightened odds of large earthquakes near Istanbul: An interaction based probability calculation, *Science,* **28,** 661–665.

Rabotnov, Y.N., 1988. *Mechanics of deformable solids,* Science, Moscow, p. 712.

Rice, J.R., 1993. Spatio-temporal complexity of slip on a fault, *J. geophys. Res.,* **98,** 9885–9907.

Rice, J.R. & Ruina, A.L., 1983. Stability of steady frictional slipping, *Trans. ASME J. Appl. Mech.,* **50,** 343–349.

Richardson, E. & Marone, C., 1999. Effects of normal stress vibrations on frictional healing, *J. geophys. Res.,* **104,** 28 859–28 878.

Ruina, A.L., 1983. Slip instability and state variable friction laws, *J. geophys. Res.,* **88,** 10 359–10 370.

Scholz, C.H., 1998. Earthquakes and friction laws, *Nature,* **391,** 37–42.

Scholz, C.H., 2002. *The mechanics of earthquakes and faulting,* 2nd edn, Cambridge University Press, Cambridge, UK, p. 435.

Sleep, N.H., 1997. Application of a unified rate and state friction theory to the mechanics of fault zones with strain localization, *J. geophys. Res.,* **102,** 2875–2895.

Sleep, N.H., 1998. Rake dependent rate and state friction, *J. geophys. Res.,* **103,** 7111–7119.

Stein, R.S., Barka, A.A. & Dieterich, J.H., 1997. Progressive failure on the North Anatolian fault since 1939 by earthquake stress triggering, *Geophys. J. Int.,* **128,** 594–604.

Stesky, R.M., Brace, W.F., Riley, D.K. & Robin, P.Y.F., 1974. Friction in faulted rocks at high temperature and pressure, *Tectonophysics,* **23,** 177–203.

Stuart, W.D. & Tullis, T.E., 1995. Fault model for preseismic deformation at Parkfield, California, *J. geophys. Res.,* **100,** 24 079–24 100.

Tse, S.T. & Rice, J.R., 1986. Crustal earthquake instability in relation to the depth variation of frictional slip properties, *J. geophys. Res.,* **91,** 9452–9472.

Turcotte, D.L., Newman, W.I. & Shcherbakov, R., 2003. Micro and macroscopic models of rock fracture, *Geophys. J. Int.,* **152,** 718–728.

Ziv, A. & Rubin, A.M., 2003. Implications of Rate-and-State Friction for Properties of Aftershock Sequence: Quasi-Static Inherently Discrete Simulations, *J. geophys Res.,* **108,** 2051, doi:10.1029/2001JB001219.

APPENDIX A: SCALING THE DUCTILE COMPLIANCE C_v

The plastic relaxation of stress in an elastic solid with damage evolution can be calculated from work and energy considerations. Neglecting energy production by creation of surface area, the work by the external forces is converted to elastic energy and plastic work. For a 1-D case, the increment of the latter is given by

$$dW^p = \tau d\varepsilon_{\rm p}, \tag{A1}$$

where the superscript p denotes contribution resulting from the plastic process and the summation convention is assumed. The dissipation is the difference between the total work and the elastic energy:

$$W^{\rm diss} = \int \tau d\varepsilon_{\rm e} - \mu\varepsilon_{\rm e}^2. \tag{A2}$$

Implicit in eq. (A2) is the assumption that all the strain is elastic. If irrecoverable strain resulting from intracrystalline processes (such as dislocation flow) is significant, it contributes an additional term to the dissipation. Differentiating eq. (A2) with respect to the elastic strain gives

$$\frac{dW^{\rm diss}}{d\varepsilon_{\rm e}} = -\varepsilon_{\rm e}^2 \frac{d\mu}{d\varepsilon_{\rm e}}, \tag{A3}$$

where we have used Hooke's law for the stress $\tau = 2\mu\varepsilon_{\rm e}$, a term that cancels the derivative of the integral on the right-hand side of

eq. (A2). Differentiating eq. (A1) with respect to the elastic strain gives

$$\frac{dW^p}{d\varepsilon_e} = \tau \frac{d\varepsilon_p}{d\varepsilon_e}. \tag{A4}$$

If all the dissipation is transferred to plastic work (neglecting surface energy production), we get an upper bound on the plastic strain by equating eqs (A3) and (A4):

$$\sigma d\varepsilon_p = -\varepsilon_e^2 d\mu. \tag{A5}$$

This expression is consistent with the expression for entropy production related to the damage process (eq. 4 in the text). The rate of plastic strain is then

$$\frac{d\varepsilon_p}{dt} = -\frac{\tau}{4\mu^2}\frac{d\mu}{dt}, \tag{A6}$$

where again we have used Hooke's law. Substituting $\alpha = 1 - \mu/\mu_0$, we have

$$\frac{d\varepsilon_p}{dt} = \frac{\tau}{4(1-\alpha)^2\mu_0}\frac{d\alpha}{dt}. \tag{A7}$$

We therefore expect proportionality between the rates of plastic strain accumulation and damage increase. This proportionality should hold even if the fraction of dissipation partitioned into surface energy is non-negligible; the rate of that dissipation fraction is expected to scale with the rate of damage increase. Comparing eq. (A7) with eq. (6), we have $C_v = [4(1-\alpha)^2\mu_0]^{-1}$. This scaling is strictly valid only if the relaxation by intracrystalline flow is negligible, a reasonable approximation for the conditions in the seismogenic zone. The scaling holds even if the fraction r of surface energy production is non-negligible; C_v in such a case would be corrected by a factor $(1 - r)$.

 doi: 10.1111/j.1365-246X.2005.02654.x

Erratum

Lyakhovsky, V., Ben-Zion, Y. & Agnon, A. 2005. A viscoelastic damage rheology and rate- and state-dependent friction (*Geophys. J. Int.,* **161,** 179–190)

In Lyakhovsky, Ben-Zion & Agnon (2005) there is an error in the captions of Figs 6 and 9. The healing rate parameters in both figure captions should be $C_1 = 10^{-12}$ 1/s, $C_2 = 0.03$.

REFERENCES

Lyakhovsky, V., Ben-Zion, Y. & Agnon, A., 2005. A viscoelastic damage rheology and rate- and state-dependent friction, *Geophys. J. Int.,* **161,** 179–190.

